

# Self-Powered 2D Material-Based pH Sensor and Photodetector Driven by Monolayer MoSe<sub>2</sub> Piezoelectric Nanogenerator

Peng Li\* and Zekun Zhang



Cite This: *ACS Appl. Mater. Interfaces* 2020, 12, 58132–58139



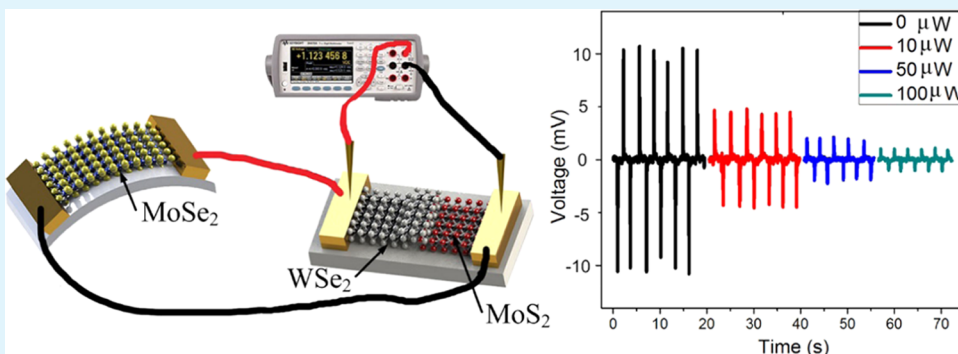
Read Online

ACCESS |

Metrics & More

Article Recommendations

Supporting Information



**ABSTRACT:** The large piezoelectricity of monolayer MoSe<sub>2</sub>, which is predicted to be stronger than that of all of the other group VIB transition-metal dichalcogenides (including MoS<sub>2</sub>), has only been theoretically investigated. Here, we report experimental evidence of in-plane piezoelectricity in MoSe<sub>2</sub>. Monolayer single-crystalline MoSe<sub>2</sub> flake derived from chemical vapor deposition demonstrates a peak output voltage of 60 mV at 0.6% strain, which is ~50% larger than that of MoS<sub>2</sub>. Piezoelectric signal along the armchair orientation of MoSe<sub>2</sub> is ~6 times larger than that along the zigzag orientation, indicative of strong anisotropic piezoelectricity. Piezoelectric nanogenerator based on a single MoSe<sub>2</sub> flake illustrates remarkable electromechanical conversion ability, and thus is able to noninvasively monitor vital health signs, such as respiratory rate and heart rate. Despite the extremely small size, MoSe<sub>2</sub> nanogenerator is able to drive pH sensor based on MoS<sub>2</sub> and photodetector based on MoS<sub>2</sub>/WSe<sub>2</sub> heterojunction due to the outstanding piezoelectricity of MoSe<sub>2</sub> and the ultralow power consumption of two-dimensional (2D) material sensors. The self-powered, solely 2D-material-based sensor units demonstrate superb sensing performance. Therefore, the discovery of piezoelectricity in monolayer MoSe<sub>2</sub> provides a route for achieving self-powered atomic-scale electromechanical systems that could stimulate further fundamental research and potential applications.

**KEYWORDS:** MoSe<sub>2</sub>, piezoelectric, nanogenerator, self-powered sensing, pH sensor, photodetector

## 1. INTRODUCTION

Two-dimensional (2D) materials have drawn significant attention in both fundamental and applied research due to their unique physical and chemical properties.<sup>1–4</sup> Their extremely large surface-to-volume ratio, exceptional electrical properties, ultralow noise level, and facile preparation make them promising candidates for sensing applications, such as ion, gas, and optical sensing.<sup>5–16</sup> Compared with traditional microelectromechanical systems (MEMS) sensors, 2D material sensors exhibit superior sensitivity, much smaller size and weight, lower energy consumption, and better flexibility.<sup>17,18</sup> However, the power supply has become the bottleneck of 2D material sensing technology. 2D material sensors reported so far exclusively rely on macroscopic external (battery) power supply, which hinders the miniaturization of the whole sensor unit. Additionally, with the rapid development of sensor networks and the Internet of things (IoT), trillions of sensor units will be needed and distributed on the earth. Replacing

charging trillions of batteries that have a limited lifetime will be impossible work. In view of the large amount of mechanical energy existing in the surrounding environment and human body, it is a promising way of utilizing piezoelectric nanogenerator<sup>19,20</sup> to harvest the energy and realize a self-powered 2D material sensor unit.

Piezoelectric materials allow reversible interconversion between mechanical energy and electrical energy.<sup>21–23</sup> Mechanical stress applied to these materials influences the electronic polarization, which results in internal electric fields

**Received:** October 7, 2020

**Accepted:** December 6, 2020

**Published:** December 16, 2020



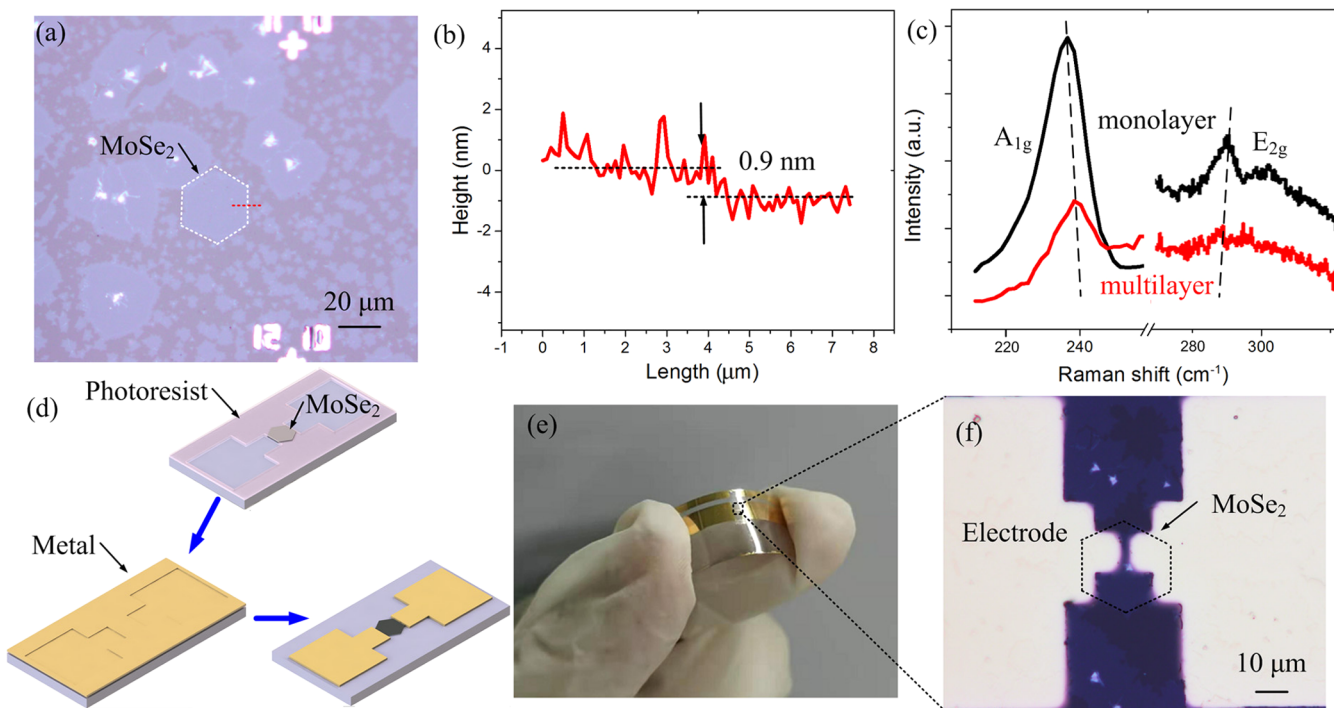


**Figure 1.** (a) Optical microscopy image of the MoSe<sub>2</sub> flakes on a PET substrate. (b) AFM height profile of a MoSe<sub>2</sub> flake extracted from a (red dash line), which demonstrates that the thickness is  $\sim 0.9$  nm. (c) Raman spectra of the CVD monolayer MoSe<sub>2</sub> and mechanically exfoliated multilayer MoSe<sub>2</sub>. (d) MoSe<sub>2</sub> piezoelectric device fabrication process. The metal electrodes are defined by photolithography, followed by metal sputtering and the lift-off process. (e) Photo of the MoSe<sub>2</sub> piezoelectric nanogenerator. (f) Optical microscopy image of the MoSe<sub>2</sub> piezoelectric nanogenerator.

and vice versa. Piezoelectric materials play an important role in a rich variety of sensors, actuators, MEMS, flexible electronics, and energy harvesting. The limitation of conventional three-dimensional (3D) piezoelectric materials, including quartz and AlN, arises due to the brittle nature.<sup>24</sup> Besides, the growing requirement for miniaturized devices calls for low-dimensional piezoelectric materials. However, one-dimensional (1D) piezoelectric materials, such as ZnO, have poor compatibility with semiconductor fabrication procedures.<sup>25,26</sup> Wang first reported the piezoelectric effect of a monolayer MoS<sub>2</sub>.<sup>27,28</sup> Since then, monolayer transition-metal dichalcogenide (M-TMD) crystals have emerged as the next-generation piezoelectric materials.<sup>28–35</sup> M-TMD crystals are able to withstand a large strain of up to 11%,<sup>36</sup> indicating that they are resistant to mechanical failure. Compared with 1D piezoelectric materials, M-TMD crystals are compatible with semiconductor fabrication procedures due to their planar structure, and the synthesis of large-area M-TMDs has been realized.<sup>37–39</sup> Density functional theory (DFT) simulation<sup>40</sup> demonstrates that both the clamped-ion and relaxed-ion piezoelectric coefficients of 2D materials exhibit a monotonic periodic trend. According to this trend, MoSe<sub>2</sub> is predicted to be the strongest in group VIB TMDs (MX<sub>2</sub>, M = Mo, W, and X = S, Se). However, most studies have focused on MoS<sub>2</sub>,<sup>41</sup> and the piezoelectricity of MoSe<sub>2</sub> has not been experimentally investigated to the best of our knowledge.

Here, we experimentally investigated the remarkable in-plane piezoelectric properties of a monolayer MoSe<sub>2</sub> for the first time. The piezoelectric output signal of the monolayer single-crystalline MoSe<sub>2</sub> was  $\sim 50\%$  larger than that of MoS<sub>2</sub>. Atomically thin nanogenerator based on MoSe<sub>2</sub> was developed, which matched the size of 2D material sensors. We used the

nanogenerator to power a pH sensor based on MoS<sub>2</sub> and a photodetector based on MoS<sub>2</sub>/WSe<sub>2</sub> heterojunction without the need for a battery power source. The self-powered sensor units composed entirely of 2D materials demonstrated superb sensing performance.

## 2. EXPERIMENTAL SECTION

A 2 in quartz tube furnace was used for the chemical vapor deposition (CVD) synthesis of monolayer single-crystalline MoSe<sub>2</sub> flakes.<sup>42</sup> The flakes were then transferred onto a flexible poly(ethylene terephthalate) (PET) substrate, which was pretreated with oxygen plasma dry etching and heated to 80 °C for 10 min during the transfer process to enhance the adhesion force between substrate and MoSe<sub>2</sub>. Tapping mode atomic force microscopy (AFM) characterization was carried out to determine the thickness of MoSe<sub>2</sub>. The MoSe<sub>2</sub> flakes were further characterized by a Witec Alpha300R Confocal Raman microscopy with an excitation laser wavelength of 532 nm. The power of the laser was below 0.5 mW to avoid sample damage. Sequentially, piezoelectric nanogenerator devices were fabricated. Due to the macroscopic continuity of MoSe<sub>2</sub>, we defined metal electrodes by regular photolithography instead of electron-beam lithography to largely reduce fabrication cost, followed by metal sputtering and lift-off process. Cr (10 nm) and Au (100 nm) were chosen as the electrodes to minimize the Schottky barrier and contact resistance. The metal electrodes on the target MoSe<sub>2</sub> flake were parallel to armchair orientation, and the gap between electrodes was 5  $\mu$ m. A Cu conductive tape or Ag paste was used to connect the electrical leads and Au electrodes. The output voltage/current of MoSe<sub>2</sub> nanogenerator was measured by a Keysight 34470A multimeter.

## 3. RESULTS AND DISCUSSION

Figure 1a shows the optical microscopy image of MoSe<sub>2</sub> flakes on the PET substrate. Hexagonal-shaped single-crystalline MoSe<sub>2</sub> domains with edges parallel to the zigzag orientation

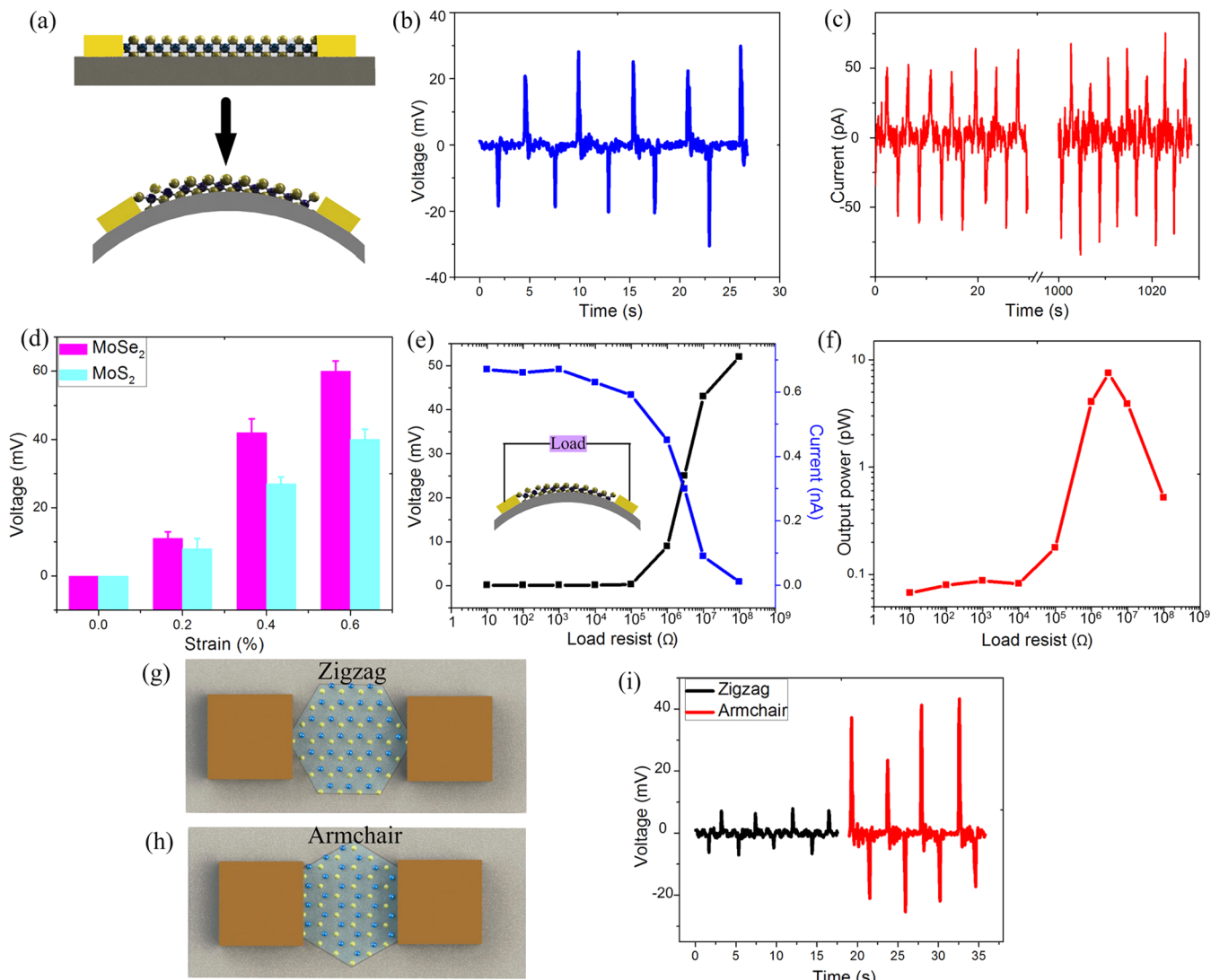


**Figure 2.** (a) Schematic diagram of the bending of the MoSe<sub>2</sub> piezoelectric nanogenerator. (b) Piezoelectric output voltage of the MoSe<sub>2</sub> piezoelectric nanogenerator under periodic bending and releasing. (c) Piezoelectric output current of the MoSe<sub>2</sub> piezoelectric nanogenerator. (d) Output voltages of the MoSe<sub>2</sub> and MoS<sub>2</sub> nanogenerators as a function of strain applied. (e) Dependence of the piezoelectric output voltage/current on load resistance. (f) Dependence of output power on load resistance. (g) Schematic view of the MoSe<sub>2</sub> piezoelectric nanogenerator with electrodes along the zigzag orientation. (h) Schematic view of the MoSe<sub>2</sub> piezoelectric nanogenerator with electrodes along the armchair orientation. (i) Piezoelectric signals of the MoSe<sub>2</sub> nanogenerator along the zigzag and armchair orientations, respectively.

were observed. Figure 1b is the AFM height profile of a typical flake extracted from Figure 1a (red dash line), which demonstrates that the thickness is  $\sim 0.9$  nm, indicating a monolayer structure.<sup>42</sup> Figure 1c exhibits the Raman spectra of a CVD monolayer MoSe<sub>2</sub> sample and mechanically exfoliated multilayer MoSe<sub>2</sub> sample. Two characteristic peaks are Raman shifts attributed to the A<sub>1g</sub> ( $\sim 239$  cm<sup>-1</sup>) and E<sub>2g</sub> ( $\sim 286$  cm<sup>-1</sup>) phonon modes of MoSe<sub>2</sub>, respectively.<sup>42</sup> The A<sub>1g</sub> peak corresponds to the out-of-plane vibration of the atoms, whereas the E<sub>2g</sub> peak corresponds to the in-plane vibration of the atoms. The A<sub>1g</sub> and E<sub>2g</sub> peaks are red-shifted and blue-shifted, respectively, from multilayer to monolayer, which is consistent with previous reports.<sup>42</sup> The sharp Raman peaks imply that the MoSe<sub>2</sub> samples studied in this work were high-quality crystals. Figure 1d demonstrates the fabrication procedure of the MoSe<sub>2</sub> piezoelectric nanogenerator. Figure 1e,f is the photo and optical microscopy image of a typical MoSe<sub>2</sub> piezoelectric nanogenerator device, respectively.

We systematically investigated the piezoelectric properties of a monolayer MoSe<sub>2</sub> for the first time. Unlike its bulk parent crystal, a monolayer MoSe<sub>2</sub> with a non-centrosymmetry structure is able to demonstrate an in-plane piezoelectric effect. As the PET substrate was bent, the monolayer MoSe<sub>2</sub> flake attached on its surface underwent uniaxial tensile/compressive strain (Figure 2a). Piezoelectric polarization charges were consequently generated at two edges of the MoSe<sub>2</sub> flake and resulted in an output voltage/current peak. When the substrate was released, a reverse charge flow led to a voltage/current peak with an opposite sign. An out-of-plane piezoelectricity in M-TMDs could be generated from a strain gradient (flexoelectricity).<sup>28,29</sup> However, in our experiment, the strain applied was along the in-plane direction, and the electric signal detected was along the in-plane direction (the electrodes were parallel to the in-plane direction). As such, the piezoelectric output properties were mainly due to the in-plane piezoelectricity. Periodic bending and releasing PET

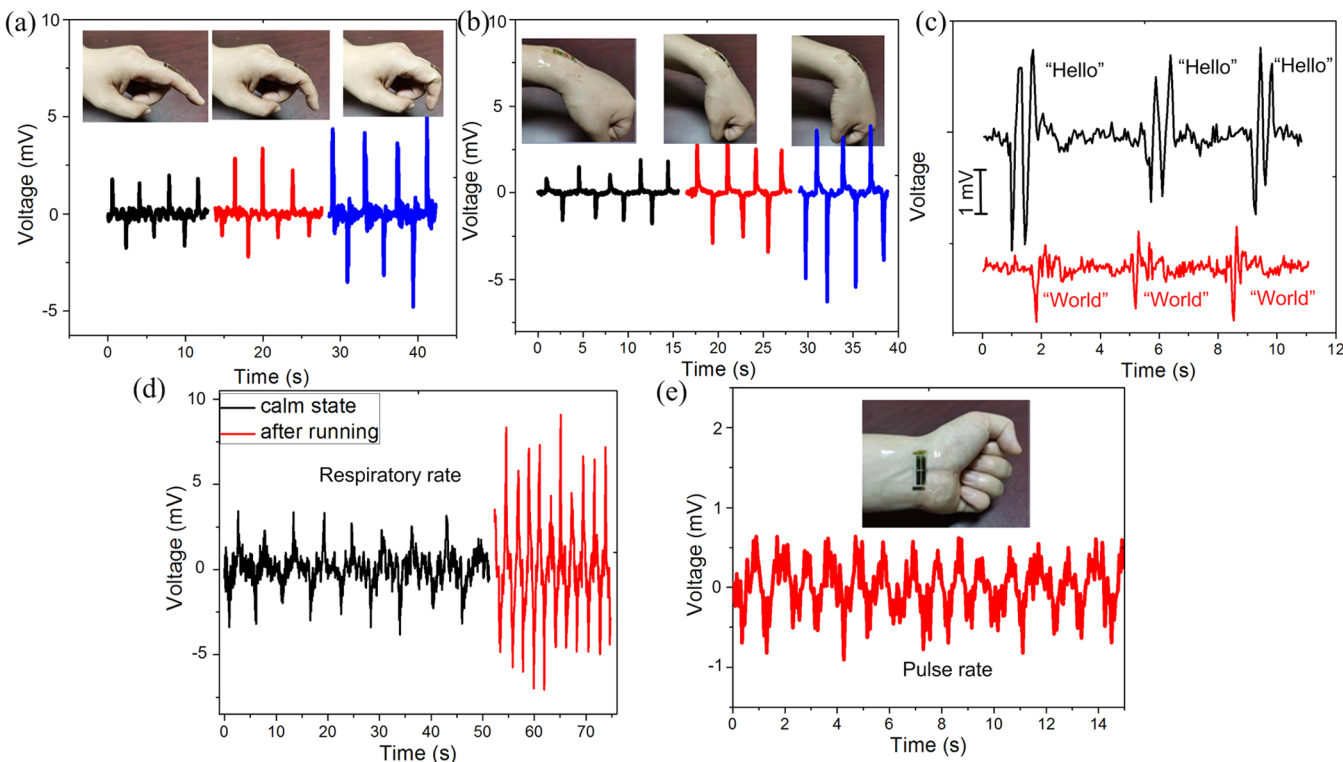


**Figure 3.** (a) Energy harvesting of the MoSe<sub>2</sub> nanogenerator from finger joint. (b) Energy harvesting of the MoSe<sub>2</sub> nanogenerator from the wrist. (c) Muscle movement during speech detected by attaching the MoSe<sub>2</sub> nanogenerator to the neck. (d) Respiratory rate detection by attaching the MoSe<sub>2</sub> nanogenerator on the chest. The frequency and amplitude of the piezoelectric signals have a significant difference when the tester is in calm state and after running. (e) Pulse rate detection by attaching the MoSe<sub>2</sub> nanogenerator on the wrist.

substrate led to periodic output voltage signals (Figure 2b) and current signals (Figure 2c). The cycle test demonstrated that the output signal of the MoSe<sub>2</sub> device was stable over a long period of operation time (Figure 2c) inasmuch as MoSe<sub>2</sub> has superb mechanical properties and is resistant to mechanical failure. The robust piezoelectricity makes MoSe<sub>2</sub> an ideal material choice for atomic-thin piezoelectric devices. No significant electrical output signal was observed from bare PET substrates without the MoSe<sub>2</sub> flake (Figure S1, Supporting Information), which further proves the piezoelectricity of MoSe<sub>2</sub>. The magnitude of the output voltage is related to the uniaxial bending strain  $\varepsilon$  applied, which can be derived from the following equation<sup>43</sup>

$$\varepsilon = h/2r \quad (1)$$

where  $h$  is the thickness of the PET substrate (150  $\mu\text{m}$ ) and  $r$  is the PET substrate bending radius. The bending strain  $\varepsilon$  was limited to 0.6% to avoid slippage between the MoSe<sub>2</sub> flake and the PET substrate. As illustrated in Figure 2d, the output voltage of a typical MoSe<sub>2</sub> device was proportional to the bending strain  $\varepsilon$ . A monolayer single-crystalline MoSe<sub>2</sub> demonstrated a peak output voltage of 60 mV at a 0.6% strain, which was ~50% larger than that of the monolayer MoS<sub>2</sub> device fabricated and tested under the same condition (Figure 1d), indicative of the outstanding piezoelectric properties of MoSe<sub>2</sub>. The reverse connection of MoSe<sub>2</sub> piezoelectric nanogenerators with the measuring equipment results in reverse output voltages (Figure S2, Supporting Information). Figure 2e,f illustrates the output characteristics of a typical MoSe<sub>2</sub> nanogenerator at 0.6% strain coupled to a load resistor. The output current reduced with an increasing load resistance value, whereas the voltage distributed on the

load resistance changed in the opposite trend. The maximum output power of the MoSe<sub>2</sub> nanogenerator reached 7.5 pW at a load resistance of ~5 M $\Omega$  (Figure 2f). According to our experimental results, the piezoelectric coefficient  $e_{11}$  of MoSe<sub>2</sub> derived is ~435 pC/m, which is close to the simulation result reported (392 pC/m).<sup>40</sup> The equivalent capacitance of MoSe<sub>2</sub> and the system is<sup>44</sup>

$$C \approx t/R \quad (2)$$

where  $t$  is the full width at half-maximum of the voltage peak and  $R$  is the load resistance. The output electrical energy in one piezoelectric discharge event is<sup>44</sup>

$$W_E = V^2 C / 2 \quad (3)$$

where  $V$  is the peak output voltage. The mechanical energy stored in the monolayer MoSe<sub>2</sub> is

$$W_M = LWE\varepsilon^2 / 2 \quad (4)$$

where  $L$  and  $W$  are the length and width of MoSe<sub>2</sub>, respectively, and  $E$  is Young's modulus of MoSe<sub>2</sub>. The efficiency of converting mechanical energy to electrical energy is

$$\eta = W_E / W_M \quad (5)$$

According to our experimental results,  $\eta \approx 7.2\%$ . The dependence of the piezoelectric response on crystal orientation was investigated. The orientations were determined by the crystal shape because the edges of the hexagonal-shaped monolayer single-crystalline MoSe<sub>2</sub> are parallel to the zigzag direction. Devices with electrodes along the armchair and zigzag orientations were fabricated and tested under the same

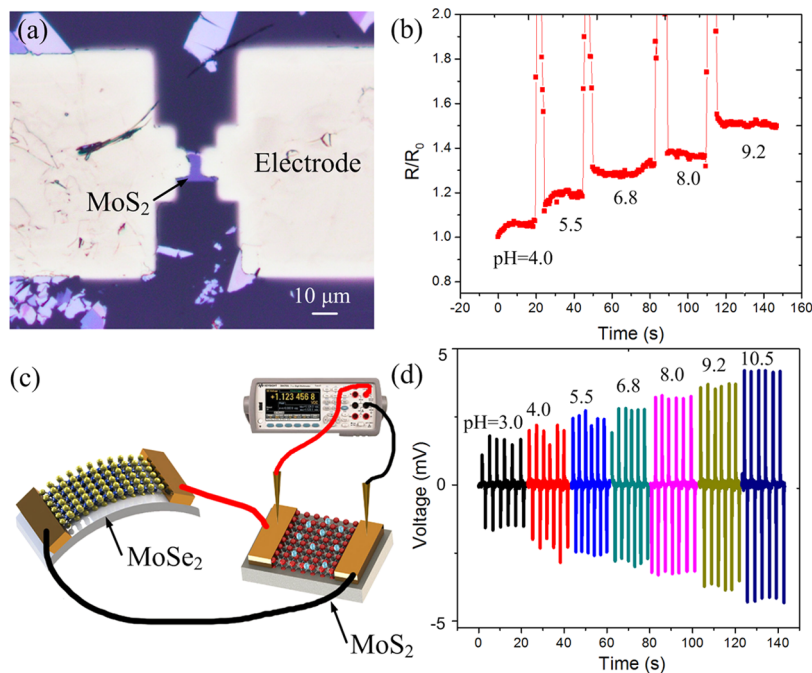


**Figure 4.** (a) Optical microscopy image of the MoS<sub>2</sub> pH sensor. (b) Dynamic resistance variation of the MoS<sub>2</sub> pH sensor. (c) Schematic view of the MoS<sub>2</sub> pH sensor driven by a MoSe<sub>2</sub> nanogenerator. (d) Sensing performance of the MoS<sub>2</sub> pH sensor driven by a MoSe<sub>2</sub> nanogenerator.

conditions (Figure 2g,h). Figure 2i clearly illustrates that the piezoelectric signals of the MoSe<sub>2</sub> nanogenerator at 0.4% strain along the armchair direction were ~6 times larger than that along the zigzag direction, indicating strong anisotropic piezoelectric properties. Therefore, the armchair is the optimum orientation for MoSe<sub>2</sub> piezoelectric devices.

Next, we explored the energy harvesting performance of the MoSe<sub>2</sub> nanogenerator from the human body. Figure 3a displays energy harvesting from finger bending by attaching the device to the tester's index finger joint. The piezoelectric output voltage is clearly enhanced as the bending degree increased from 30 to 90°. The device was then attached to the tester's wrist, and piezoelectric signals were also observed with magnitudes proportional to the wrist bending angles (Figure 3b). Therefore, the MoSe<sub>2</sub> piezoelectric device holds great potential in human activity monitoring. The MoSe<sub>2</sub> nanogenerator was attached to the neck of the tester to noninvasively monitor muscle movement during speech (Figure 3c). The obtained V-t curves were clearly different when the tester pronounced different words, such as "hello" and "world". The waveforms illustrated similar characteristic peaks when the tester spoke the same word, indicative of good repeatability. It brings promise for the remote control of human/machine interfaces. Next, we demonstrated prototype wearable MoSe<sub>2</sub> devices that are capable of noninvasively monitoring vital health signs, such as respiratory rate and heart rate. The MoSe<sub>2</sub> nanogenerator was applied to monitor the respiratory rate by attaching it to the chest of the tester. Figure 3d depicts the obtained V-t curves when the tester was in a calm state and right after running, respectively. Both the frequency and amplitude of the piezoelectric signal related to respiration significantly increased due to high-intensity exercise. MoSe<sub>2</sub> nanogenerator can monitor pulse rate by attaching it to the tester's wrist (Figure 3e). The magnitude of the piezoelectric signal was ~0.7 mV, and the pulse rate extracted was ~60/min. Therefore, the MoSe<sub>2</sub> piezoelectric

device holds great potential in health-tracking wearable devices.<sup>45–48</sup>

After demonstrating the MoSe<sub>2</sub> nanogenerator's remarkable electromechanical conversion ability, we used the nanogenerator to drive a pH sensor based on MoS<sub>2</sub>. Figure 4a is the optical microscopy image of a MoS<sub>2</sub> sensor. AFM characterization demonstrated that the thickness of the mechanically exfoliated multilayer MoS<sub>2</sub> flake was ~15 nm. Solutions with different pH values were sequentially introduced onto the MoS<sub>2</sub> sensor at room temperature. The resistance of the MoS<sub>2</sub> sensor measured by a Keysight 34470A multimeter rapidly increased as the pH value changed from 4.0 to 9.2 (Figure 4b). This process was repeated several times and demonstrated good repeatability (Figure S3, Supporting Information). The response rate of our MoS<sub>2</sub> pH sensor extracted was less than 10 s, which is mainly attributed to the superb electrical properties and large surface–volume ratio of MoS<sub>2</sub>. The pH sensing mechanism of the MoS<sub>2</sub> sensor was investigated. The I-V characteristic curve of a typical MoS<sub>2</sub> device demonstrates good linearity (Figure S4, Supporting Information), indicative of an insignificant Schottky barrier between MoS<sub>2</sub> and Cr/Au metal electrodes.<sup>41,42</sup> Therefore, the output signals are mainly attributed to the MoS<sub>2</sub> flake instead of metal contact during sensing. The resistivity of MoS<sub>2</sub> can be expressed by the equation

$$\rho = 1/nqu \quad (6)$$

where  $\rho$  is the resistivity,  $n$  is the electron density,  $q$  is the charge per carrier, and  $u$  is the carrier mobility. MoS<sub>2</sub> is a n-type semiconductor, so negatively charged electrons are majority carriers. The OH<sup>-</sup> ion adsorption serves as a negative gate voltage, which reduces the electron density  $n$  in MoS<sub>2</sub> and results in larger resistivity. In contrast, the H<sup>+</sup> ion adsorption increases the electron density and reduces the resistivity. We used the MoSe<sub>2</sub> nanogenerator to power the MoS<sub>2</sub> pH sensor by connecting them in series to form a loop (Figure 4c). A

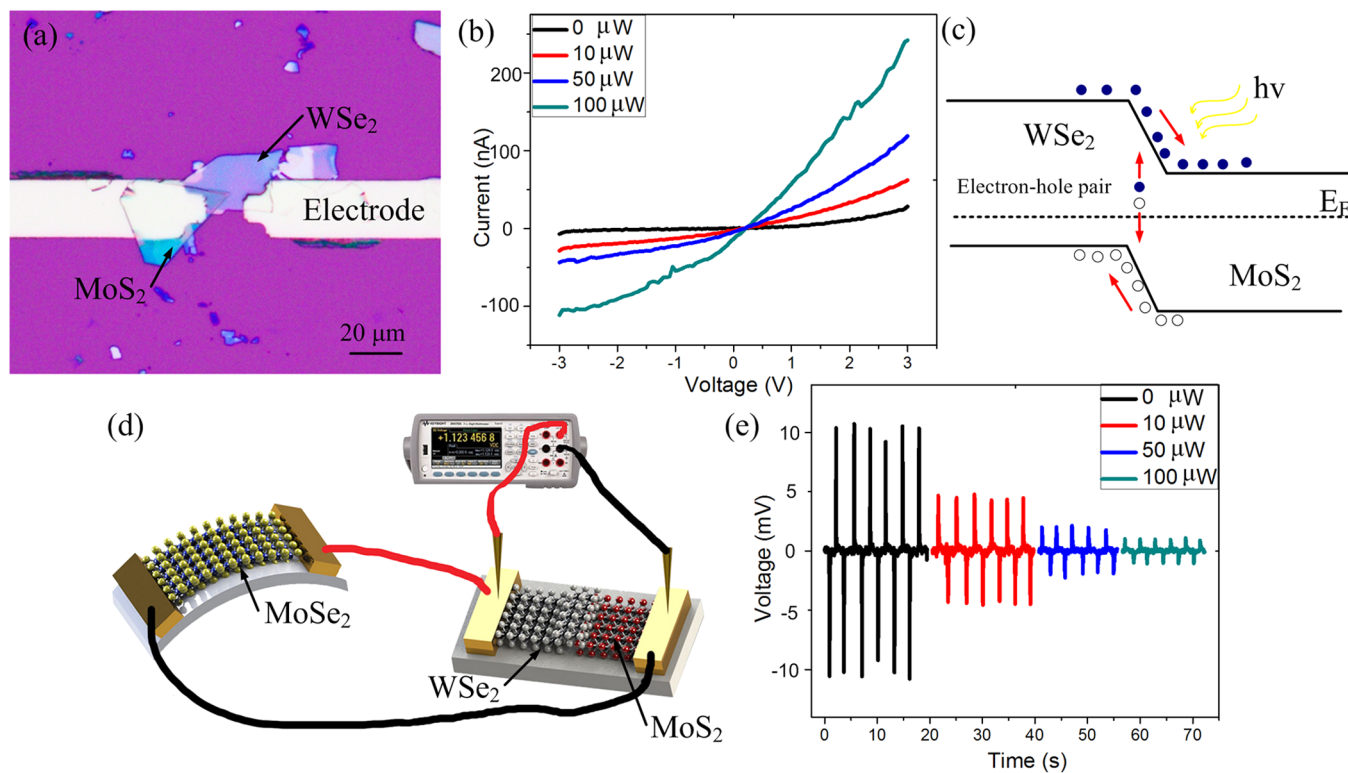


**Figure 5.** (a) Optical microscopy image of the MoS<sub>2</sub>/WSe<sub>2</sub> heterojunction photodetector. (b)  $I$ – $V$  curves of the MoS<sub>2</sub>/WSe<sub>2</sub> heterojunction under different intensities of illumination. (c) Energy band structure of the MoS<sub>2</sub>/WSe<sub>2</sub> heterojunction under illumination. (d) Schematic view of the MoS<sub>2</sub>/WSe<sub>2</sub> heterojunction photodetector driven by MoSe<sub>2</sub> nanogenerator. (e) Sensing performance of the MoS<sub>2</sub>/WSe<sub>2</sub> heterojunction photodetector driven by a MoSe<sub>2</sub> nanogenerator.

clear sensitivity to pH change was observed (Figure 4d). As the pH value changed from 3.0 to 10.5, the resistance of the MoS<sub>2</sub> sensor increased and the voltage across the MoS<sub>2</sub> sensor varied from 1.6 to 4.2 mV accordingly. As such, the self-powered MoS<sub>2</sub> pH sensor driven by the MoSe<sub>2</sub> nanogenerator demonstrated good sensing performance without a need for a battery power source. Due to the extremely small size of the MoSe<sub>2</sub> nanogenerator and MoS<sub>2</sub> sensor, we successfully integrated them on a 1 cm × 1 cm PET substrate. The integrated self-powered sensing unit illustrated the same pH sensing performance as depicted in Figure 4d.

The 2D material heterojunction is another fundamental device building block for sensing the applications. The MoS<sub>2</sub>/WSe<sub>2</sub> photodetector was chosen as a typical 2D material heterojunction sensor. Figure 5a is the optical microscopy image of a MoS<sub>2</sub>/WSe<sub>2</sub> atomically thin vertical heterojunction. Multilayer MoS<sub>2</sub> and WSe<sub>2</sub> flakes were both derived from mechanical exfoliation. We used a white light source to illuminate the photodetector, and the estimated optical power distributed on the heterojunction was 10, 50, and 100 μW, respectively. The  $I$ – $V$  characteristic curves derived by an Agilent B1500A semiconductor parameter analyzer demonstrated that the current of the MoS<sub>2</sub>/WSe<sub>2</sub> heterojunction drastically increased under illumination (Figure 5b). The photoresponsivity acquired was 1.9 mA/W. As the light was turned off, the current of the MoS<sub>2</sub>/WSe<sub>2</sub> heterojunction rapidly changed back to the original value. This process was repeated several times and demonstrated good repeatability. The illumination results in photon absorption and the excitation of electron–hole pairs in the heterojunction region, which can be extracted by applying a bias (Figure 5c). As such,

the MoS<sub>2</sub>/WSe<sub>2</sub> heterostructure converts the energy of photon absorbed into photocurrent, and its resistivity reduces accordingly. Compared with a photodetector based on a single 2D material, this heterojunction structure largely increases sensitivity by separating the photogenerated electron–hole pairs, which results in enhanced carrier lifetime and photoresponsivity. We used the MoSe<sub>2</sub> nanogenerator to power the MoS<sub>2</sub>/WSe<sub>2</sub> photodetector (Figure 5d). The voltage across the MoS<sub>2</sub>/WSe<sub>2</sub> heterojunction drastically decreased from 10 to 1.2 mV as the illumination intensity varied from 0 to 100 μW, inasmuch as the resistance of heterojunction reduced significantly (Figure 5e). Therefore, the self-powered 2 material heterojunction photodetector driven by a MoSe<sub>2</sub> nanogenerator demonstrated superb sensing performance without the need of a battery power source.

#### 4. CONCLUSIONS

We systematically investigated the remarkable in-plane piezoelectric properties of a monolayer MoSe<sub>2</sub> for the first time. Monolayer single-crystalline MoSe<sub>2</sub> demonstrated a peak output voltage of 60 mV at 0.6% strain, which was ~50% larger than that of MoS<sub>2</sub>. MoSe<sub>2</sub> illustrated a strong anisotropic piezoelectric response. The piezoelectric signal along the armchair direction was ~6 times larger than that along the zigzag direction. We used a MoSe<sub>2</sub> nanogenerator to drive a MoS<sub>2</sub> pH sensor and a MoS<sub>2</sub>/WSe<sub>2</sub> photodetector, respectively, by harvesting ambient mechanical energy without a need for a battery power source. Our research offers a platform for the fundamental investigation of electronic polarization and electromechanical conversion in 2D piezoelectric materials and

provides a route for achieving novel self-powered atomic-scale electromechanical systems.

## ■ ASSOCIATED CONTENT

### SI Supporting Information

The Supporting Information is available free of charge at <https://pubs.acs.org/doi/10.1021/acsami.0c18028>.

Output properties of bare PET substrate without MoSe<sub>2</sub>, switching polarity test of MoSe<sub>2</sub> piezoelectric nanogenerators, repeatability of the MoS<sub>2</sub> pH sensor, *I*–*V* characteristic of the MoS<sub>2</sub> sensor, CVD synthesis of MoSe<sub>2</sub>, MoS<sub>2</sub> pH sensor, and MoS<sub>2</sub>/WSe<sub>2</sub> photodetector fabrication procedure ([PDF](#))

## ■ AUTHOR INFORMATION

### Corresponding Author

Peng Li – State Key Laboratory of Precision Measurement Technology and Instruments, Department of Precision Instruments, Tsinghua University, Beijing 100084, China;  
✉ [orcid.org/0000-0002-8791-7465](https://orcid.org/0000-0002-8791-7465); Email: [pengl@mail.tsinghua.edu.cn](mailto:pengl@mail.tsinghua.edu.cn)

### Author

Zekun Zhang – State Key Laboratory of Precision Measurement Technology and Instruments, Department of Precision Instruments, Tsinghua University, Beijing 100084, China

Complete contact information is available at:

<https://pubs.acs.org/10.1021/acsami.0c18028>

### Notes

The authors declare no competing financial interest.

## ■ ACKNOWLEDGMENTS

This work was supported by the National Natural Science Foundation of China (51775306) and the Beijing Municipal Natural Science Foundation (4192027).

## ■ REFERENCES

- (1) Taniguchi, T.; Nurdwijayanto, L.; Li, S.; Lim, H. E.; Miyata, Y.; Lu, X.; Ma, R.; Tang, D. M.; Ueda, S.; Tsukagoshi, K.; Sasaki, T.; Osada, M. On/Off Boundary of Photocatalytic Activity Between Single- and Bilayer MoS<sub>2</sub>. *ACS Nano* **2020**, *14*, 6663–6672.
- (2) Lee, C.; Wei, X. D.; Kysar, J. W.; Hone, J. Measurement of the Elastic Properties and Intrinsic Strength of Monolayer Graphene. *Science* **2008**, *321*, 385–388.
- (3) Huang, Z.; Han, W.; Tang, H.; Ren, L.; Chander, D. S.; Qi, X.; Zhang, H. Photoelectrochemical-Type Sunlight Photodetector Based on MoS<sub>2</sub>/Graphene Heterostructure. *2D Mater.* **2015**, *2*, No. 035011.
- (4) Cha, E.; Patel, M. D.; Park, J.; Hwang, J.; Prasad, V.; Cho, K.; Choi, W. 2D MoS<sub>2</sub> as an Efficient Protective Layer for Lithium Metal Anodes in High-Performance Li-S Batteries. *Nat. Nanotechnol.* **2018**, *13*, 337–344.
- (5) Ohno, Y.; Maehashi, K.; Yamashiro, Y.; Matsumoto, K. Electrolyte-Gated Graphene Field-Effect Transistor for Detecting pH Protein Adsorption. *Nano Lett.* **2009**, *9*, 3318–3322.
- (6) Ang, P. K.; Chen, W.; Wee, A. T. S.; Loh, K. P. Solution-Gated Epitaxial Graphene as pH Sensor. *J. Am. Chem. Soc.* **2008**, *130*, 14392–14393.
- (7) Kuila, T.; Bose, S.; Khanra, P.; Mishra, A. K.; Kim, N. H.; Lee, J. H. Recent Advances in Graphene-Based Biosensors. *Biosens. Bioelectron.* **2011**, *26*, 4637–4648.
- (8) Maity, A.; Sui, X.; Pu, H.; Bottum, K. J.; Jin, B.; Chang, J.; Zhou, G.; Lu, G.; Chen, J. Sensitive Field-Effect Transistor Sensors with Atomically Thin Black Phosphorus Nanosheets. *Nanoscale* **2020**, *12*, 1500–1512.
- (9) Li, P.; Zhang, D.; Liu, J.; Chang, H.; Sun, Y.; Yin, N. Air-Stable Black Phosphorus Devices for Ion Sensing. *ACS Appl. Mater. Interfaces* **2015**, *7*, 24396–24402.
- (10) Lee, K.; Gatensby, R.; McEvoy, N.; Hallam, T.; Duesberg, G. S. High-Performance Sensors Based on Molybdenum Disulfide Thin Films. *Adv. Mater.* **2013**, *25*, 6699–6702.
- (11) Liu, Z.; Huang, J.; Wang, Q.; Zhou, J.; Ye, J.; Li, X.; Geng, Y.; Liang, Z.; Du, Y.; Tian, X. Indium Oxide-Black Phosphorus Composites for Ultrasensitive Nitrogen Dioxide Sensing at Room Temperature. *Sens. Actuators, B* **2020**, *308*, No. 127650.
- (12) Zhang, D.; Yang, Z.; Li, P.; Pang, M.; Xue, Q. Flexible Self-powered High-Performance Ammonia Sensor Based on Au-Decorated MoSe<sub>2</sub> Nanoflowers Driven by Single Layer MoS<sub>2</sub>-Flake Piezoelectric Nanogenerator. *Nano Energy* **2019**, *65*, No. 103974.
- (13) Zhao, J.; Li, N.; Yu, H.; Wei, Z.; Liao, M.; Chen, P.; Wang, S.; Shi, D.; Sun, Q.; Zang, G. Highly Sensitive MoS<sub>2</sub> Humidity Sensor Array for Noncontact Sensation. *Adv. Mater.* **2017**, *29*, No. 1702076.
- (14) Late, D. J.; Huang, Y. K.; Liu, B.; Acharya, J.; Shirodkar, S. N.; Luo, J. J.; Yan, A. M.; Charles, D.; Waghmare, U. V.; David, V. P.; Rao, C. N. R. Sensing Behavior of Atomically Thin-Layered MoS<sub>2</sub> Transistors. *ACS Nano* **2013**, *7*, 4879–4891.
- (15) Singh, E.; Singh, P.; Kim, K. S.; Yeom, G. Y.; Nalwa, H. S. Flexible Molybdenum Disulfide (MoS<sub>2</sub>) Atomic Layers for Wearable Electronics and Optoelectronics. *ACS Appl. Mater. Interfaces* **2019**, *11*, 11061–11105.
- (16) Nalwa, H. S. A Review of Molybdenum Disulfide (MoS<sub>2</sub>) Based Photodetectors: from Ultra-Broadband, Self-Powered to Flexible Devices. *RSC Adv.* **2020**, *10*, 30529–30602.
- (17) Kim, J. H.; Mirzaei, A.; Kim, H. W.; Kim, S. S. Flexible and Low Power CO Gas Sensor with Au-Functionalized 2D WS<sub>2</sub> Nanoflakes. *Sens. Actuators, B* **2020**, *313*, No. 128040.
- (18) He, Q.; Zeng, Z.; Yin, Z.; Li, H.; Wu, X.; Huang, X.; Zhang, H. Fabrication of Flexible MoS<sub>2</sub> Thin-Film Transistor Arrays for Practical Gas-Sensing Applications. *Small* **2012**, *8*, 2994–2999.
- (19) Park, K. I.; Xu, S.; Liu, Y.; Hwang, G. T.; Kang, S. J. L.; Wang, Z. L.; Lee, K. J. Piezoelectric BaTiO<sub>3</sub> Thin Film Nanogenerator on Plastic Substrates. *Nano Lett.* **2010**, *10*, 4939–4943.
- (20) Huang, T.; Wang, C.; Yu, H.; Wang, H. Z.; Zhang, Q. H.; Zhu, M. F. Human Walking-Driven Wearable All-Fiber Triboelectric Nanogenerator Containing Electrospun Polyvinylidene Fluoride Piezoelectric Nanofibers. *Nano Energy* **2015**, *14*, 226–235.
- (21) Dong, K.; Peng, X.; Wang, Z. L. Fiber/Fabric-Based Piezoelectric and Triboelectric Nanogenerators for Flexible/Stretchable and Wearable Electronics and Artificial Intelligence. *Adv. Mater.* **2020**, *32*, No. 1902549.
- (22) Zhang, S.; Liu, Z. F.; Ruan, M. N.; Guo, Z. G.; Lei, E.; Zhao, W.; Zhao, D.; Wu, X.; Chen, D. Enhanced Piezoelectric-Effect-Assisted Photoelectrochemical Performance in ZnO Modified with Dual Cocatalysts. *Appl. Catal., B* **2020**, *262*, No. 118279.
- (23) Jung, Y. H.; Hong, S. K.; Wang, H. S.; Han, J. H.; Pham, T. X.; Park, H.; Kim, J.; Kang, S.; Yoo, C. D.; Lee, K. J. Flexible Piezoelectric Acoustic Sensors and Machine Learning for Speech Processing. *Adv. Mater.* **2020**, *32*, No. 1904020.
- (24) Gablech, I.; Klempa, J.; Pekarek, J.; Vyroubal, P.; Hrabina, J.; Hola, M.; Kunz, J.; Brodsky, J.; Neuzil, P. Simple and Efficient AlN-Based Piezoelectric Energy Harvesters. *Micromachines* **2020**, *11*, No. 143.
- (25) Jin, C.; Hao, N. J.; Xu, Z.; Trase, I.; Nie, Y.; Dong, L.; Closson, A.; Chen, Z.; Zhang, J. X. J. Flexible Piezoelectric Nanogenerators Using Metal-Doped ZnO-PVDF Films. *Sens. Actuators, A* **2020**, *305*, No. UNSP 111912.
- (26) Le, A. T.; Ahmadipour, M.; Pung, S. Y. A Review on ZnO-Based Piezoelectric Nanogenerators: Synthesis, Characterization Techniques, Performance Enhancement and Applications. *J. Alloys Compd.* **2020**, *844*, No. 156172.
- (27) Wu, W.; Wang, L.; Li, Y.; Zhang, F.; Lin, L.; Niu, S.; Chenet, D.; Zhang, X.; Hao, Y.; Heinz, T. F.; Hone, J.; Wang, Z. L.

- Piezoelectricity of Single-Atomic-layer MoS<sub>2</sub> for Energy Conversion and Piezotronics. *Nature* **2014**, *514*, 470–474.
- (28) Kang, S.; Jeon, S.; Kim, S.; Seol, D.; Yang, H.; Lee, J.; Kim, Y. Tunable Out-of-Plane Piezoelectricity in Thin-Layered MoTe<sub>2</sub> by Surface Corrugation-Mediated Flexoelectricity. *ACS Appl. Mater. Interfaces* **2018**, *10*, 27424–27431.
- (29) Seo, J.; Kim, Y.; Park, W. Y.; Son, J. Y.; Jeong, C. K.; Kim, H.; Kim, W. H. Out-of-Plane Piezoresponse of Monolayer MoS<sub>2</sub> on Plastic Substrates Enabled by Highly Uniform and Layer-Controllable CVD. *Appl. Surf. Sci.* **2019**, *487*, 1356–1361.
- (30) Lee, J. H.; Park, J. Y.; Cho, E. B.; Kim, T. Y.; Han, S. A.; Kim, T. H.; Liu, Y.; Kim, S. K.; Roh, C. J.; Yoon, H. J.; Ryu, H.; Seung, W.; Lee, J. S.; Lee, J.; Kim, S. W. Reliable Piezoelectricity in Bilayer WSe<sub>2</sub> for Piezoelectric Nanogenerators. *Adv. Mater.* **2017**, *29*, No. 1606667.
- (31) Kim, J.; Lee, E.; Bhoyate, S.; An, T. K. Stable and High-Performance Piezoelectric Sensor via CVD Grown WS<sub>2</sub>. *Nanotechnology* **2020**, *31*, No. 445203.
- (32) Yu, S.; Rice, Q.; Tabibi, B.; Li, Q.; Seo, F. J. Piezoelectricity in WSe<sub>2</sub>/MoS<sub>2</sub> Heterostructure Atomic Layers. *Nanoscale* **2018**, *10*, 12472–12479.
- (33) Lee, G. J.; Lee, M. J.; Park, J. J.; Hyeon, D. Y.; Jeong, C. K.; Park, K. I. Piezoelectric Energy Harvesting from Two-Dimensional Boron Nitride Nanoflakes. *ACS Appl. Mater. Interfaces* **2019**, *11*, 37920–37926.
- (34) Peng, Y.; Que, M.; Tao, J.; Wang, X.; Lu, J.; Hu, G.; Wan, B.; Xu, Q.; Pan, C. Progress in Piezotronic and Piezo-Phototronic Effect of 2D Materials. *2D Mater.* **2018**, *5*, No. 042003.
- (35) Maity, K.; Mahanty, B.; Sinha, T. K.; Garain, S.; Biswasm, A.; Ghosh, S. K.; Manna, S.; Ray, S. K.; Mandal, D. Two-Dimensional Piezoelectric MoS<sub>2</sub>-Modulated Nanogenerator and Nanosensor Made of Poly(vinylidene fluoride) Nanofiber Webs for Self-Powered Electronics. *Energy Technol.* **2017**, *5*, 234–243.
- (36) Bertolazzi, S.; Brivio, J.; Kis, A. Stretching and Breaking of Ultrathin MoS<sub>2</sub>. *ACS Nano* **2011**, *5*, 9703–9709.
- (37) Zhan, Y.; Liu, Z.; Najmaei, S.; Ajayan, P. M.; Lou, J. Large-Area Vapor-Phase Growth and Characterization of MoS<sub>2</sub> Atomic Layers on a SiO<sub>2</sub> Substrate. *Small* **2012**, *8*, 966–971.
- (38) Gao, Y.; Liu, Z.; Sun, D. M.; Huang, L.; Ma, L. P.; Yin, L. C.; Ma, T.; Zhang, Z.; Ma, X. L.; Peng, L. M.; Cheng, H. M.; Ren, W. Large-Area Synthesis of High-Quality and Uniform Monolayer WS<sub>2</sub> on Reusable Au Foils. *Nat. Commun.* **2015**, *6*, No. 8569.
- (39) Zhang, W.; Chiu, M. H.; Chen, C. H.; Chen, W.; Li, L. J.; Wee, A. T. S. Role of Metal Contacts in High-Performance Phototransistors Based on WSe<sub>2</sub> Monolayers. *ACS Nano* **2014**, *8*, 8653–8661.
- (40) Duerloo, K.-A. N.; Ong, M. T.; Reed, E. J. Intrinsic Piezoelectricity in Two-Dimensional Materials. *J. Phys. Chem. Lett.* **2012**, *3*, 2871–2876.
- (41) Manzeli, S.; Allain, A.; Ghadimi, A.; Kis, A. Piezoresistivity and Strain-Induced Band Gap in Atomically Thin MoS<sub>2</sub>. *Nano Lett.* **2015**, *15*, 5330–5335.
- (42) Lu, X.; Utama, I. B.; Lin, J.; Gong, X.; Zhang, J.; Zhao, Y.; Pantelides, S. T.; Wang, J.; Dong, Z.; Liu, Z.; Zhou, W.; Xiong, Q. Large-Area Synthesis of Monolayer and Few-Layer MoSe<sub>2</sub> Films on SiO<sub>2</sub> Substrates. *Nano Lett.* **2014**, *14*, 2419–2425.
- (43) Li, P.; Zhang, D.; Wu, J.; Cao, Y.; Wu, Z. Flexible Integrated Black Phosphorus Sensor Arrays for High Performance Ion Sensing. *Sens. Actuators, B* **2018**, *273*, 358–364.
- (44) Wang, Z. L.; Song, J. Piezoelectric Nanogenerators Based on Zinc Oxide Nanowire Arrays. *Science* **2006**, *312*, 242–246.
- (45) Ma, Z.; Li, S.; Wang, H.; Cheng, W.; Li, Y.; Pan, L.; Shi, Y. Advanced Electronic Skin Devices for Healthcare Applications. *J. Mater. Chem. B* **2019**, *7*, 173–197.
- (46) Ghosh, S. K.; Adhikary, P.; Jana, S.; Biswas, A.; Sencadas, V.; Gupta, S. D.; Tudu, B.; Mandal, D. Electrospun Gelatin Nanofiber Based Self-Powered Bio-E-Skin for Health Care Monitoring. *Nano Energy* **2017**, *36*, 166–175.
- (47) Liu, Y.; Zheng, H.; Zhao, L.; Liu, S.; Yao, K.; Li, D.; Yiu, C.; Gao, S.; Avila, R.; Pakpong, C.; Chang, L.; Wang, Z.; Huang, X.; Xie, Z.; Yang, Z.; Yu, X. Electronic Skin from High-Throughput Fabrication of Intrinsically Stretchable Lead Zirconate Titanate Elastomer. *Research* **2020**, *2020*, No. 1085417.
- (48) Maity, K.; Garain, S.; Henkel, K.; Schmeiber, D.; Mandal, D. Self-Powered Human Health Monitoring Through Aligned PVDF Nanofibers Interfaces Skin-Interactive Piezoelectric Sensor. *ACS Appl. Polym. Mater.* **2020**, *2*, 862–878.